Journal of Fluids Engineering. Received October 11, 2017;
Accepted manuscript posted November 15, 2018. doi:10.1115/1.4041985

Experimental analysis of cavitation phenomena on Kaplan turbine blades using flow visualization

Andrej Podnar

University of Ljubljana, Faculty of Mechanical Engineering, Aškerčeva 6, SI 1000 Ljubljana, Slovenia

andrej.podnar@gmail.com

Matevž Dular

University of Ljubljana, Faculty of Mechanical Engineering, Aškerčeva 6, SI 1000 Ljubljana, Slovenia

matevz.dular@fs.uni-lj.si

Brane Širok

University of Ljubljana, Faculty of Mechanical Engineering, Aškerčeva 6, SI 1000 Ljubljana, Slovenia

brane.sirok@fs.uni-lj.si

Journal of Fluids Engineering. Received October 11, 2017;
Accepted manuscript posted November 15, 2018. doi:10.1115/1.4041985

Marko Hočevar[1]

University of Ljubljana, Faculty of Mechanical Engineering, Aškerčeva 6, SI 1000 Ljubljana, Slovenia

marko.hocevar@fs.uni-lj.si

ABSTRACT

In this study, a comparison of two different Kaplan turbine runners with differently shaped turbine blades was performed. The two turbines differed in the selection of the hydrofoil, the main hydrofoil parameters of which had been modified including, the position of maximum thickness and curvature and the inlet edge radius. Both turbines (unmodified and modified hydrofoils) were tested on a rig designed for low pressure model turbine acceptance tests. The effect of blade shape on cavitation inception, development and intensity was demonstrated using computer aided visualization. Visualization was performed on the suction side of Kaplan runner blade where the shape of the blade determines cavitation inception and development. The modified Kaplan turbine reduced the cavitation phenomena, and as a result, both turbine performance and output increased for the selected operating points. This demonstrates that choosing the right turbine blade shape is key for optimal turbine performance.

[1] Corresponding author: Marko Hočevar

Journal of Fluids Engineering. Received October 11, 2017;
Accepted manuscript posted November 15, 2018. doi:10.1115/1.4041985

1 INTRODUCTION

Hydropower plants are the most important source of renewable energy. Water turbines with single-regulation using guide vanes are most efficient at the design point. Here, the best combination of runner speed, pump head and discharge is achieved. At the design condition, i.e., the so-called best efficiency point, flow separation is low and cavitation is usually not present. Kaplan turbines offer double regulation and can operate over a broad range of operating parameters with high efficiency compared to single regulated turbines.

Hydropower was originally designed as a source of base load electricity generation, but now it is mostly used to balance grid fluctuations as a consequence of market deregulation and the introduction of other renewable energy resources [1]. New water turbine designs must, therefore, account for this type of operation and achieve a high efficiency away from their optimal operating point. While Kaplan turbines are suitable for such operation, challenges remain to reduce the detrimental effect that cavitation has on turbine performance while maintaining optimal performance over the widest operating range [2].

Although much research has been done in improving all hydraulic turbine types, the gains in efficiency can be measured in tenths of a percent. Nevertheless, the presence of cavitation phenomena in water turbines remains problematic. It has been demonstrated that the presence of cavitation decreases turbine efficiency, increases turbine vibrations and blade wear all of which reduce the operating life of the turbine [3, 4, 5].

There is a thin line between high efficiency and cavitation development on a turbine blade. A pressure difference between the suction and pressure sides of the blade enables energy transfer, which is limited by cavitation. If the flow velocity is too high, the pressure on the suction side will drop below the vapor pressure. Cavitation on the runner blades then appears at various locations, such as on the leading edge of the turbine blade, on the blade root, at the tip edge, in the gap between the tip of the blade and the discharge ring, on the suction side of the blade near the trailing edge and behind the blade in the draft tube cone [6]. At all these locations cavitation is triggered because of the turbine’s suboptimal operating conditions and suboptimal runner blade geometry.

Several studies using visualization were performed in the past to study cavitation in hydraulic turbine machinery [7, 8].

Based on our previous experience of the Kaplan turbine design, cavitation most commonly occurs at the tip, i.e., at the location having the highest peripheral speed [7]. In this paper, we present a study on the profile modification of Kaplan turbine blades to either prevent or delay cavitation inception and development during different operating regimes. Additionally, we present the background and how modifications to the runner blades were made. Finally, we show how the modified runner blades perform better than the unmodified blades in terms of turbine output and reduced cavitation occurrence.

2 KAPLAN TURBINE BLADE GEOMETRY MODIFICATIONS

The shape of the Kaplan runner blade is of paramount importance for flow kinematics in the runner. Blade optimization reduces the inception and the development of cavitation on the runner blades. When the Kaplan runner blade geometry is designed, analyzed or reshaped, successive turbine blade profiles from the runner hub towards the outer edge can be drawn. The denser the turbine blade profiles are drawn, the more precise a representation of the turbine blade shape becomes. The turbine blade profiles, therefore, represent the basic building blocks of each blade (Figure 1). To modify the entire Kaplan turbine, all the turbine blade profiles must be geometrically reshaped, resulting in a spatially redesigned Kaplan runner blade. Optimal turbine blade profiles will result in a blade that is optimized for maximum hydraulic efficiency, minimum turbine vibrations and reduced cavitation phenomena. In this study, we focus on high volume flow rates on the right-hand side of the hill diagram, where cavitation frequently occurs.

Since different types of cavitation on the Kaplan runner blades exist, we also focus on the cavitation that occurs near the tip where cavitation often starts. Figure 1 (blue) shows the unmodified turbine blade profile of the blade near the tip at 95% of the nominal turbine diameter *D*. The extracted turbine blade profile was drawn in a Cartesian x-y coordinate system (red) before being transformed into cylindrical

Journal of Fluids Engineering. Received October 11, 2017;
Accepted manuscript posted November 15, 2018. doi:10.1115/1.4041985

coordinate system (blue). This turbine blade profile is denoted in the following text as the unmodified profile.

There are many known families of turbine blade profiles, namely NACA (Series 4 to 8), Götingen, Munk, NPL, NASA and others [9, 10]. This enables the turbine designer to select and possibly modify the blade's hydrofoil shape according to specific operating conditions, for instance for operation at high volume flow rates and high runner blade angles.

Every turbine blade profile features important geometrical parameters that determine flow characteristics. The most important are (Figure 2) the leading edge radius, the shape of the mean camber line, profile thickness and curvature, the position of maximum thickness, the position of maximum curvature and the trailing edge shape [11].

The shape and dimension of the blade's leading edge determines how the flow streamlines pass the leading edge and continue down the profile. The aim is to design a leading edge such that the flow streamlines can pass smoothly and create as little flow separation as possible. Sharp edges are not optimal because they increase energy (pressure) dissipation within the flow [11]. An obvious choice is to round the leading edges on the hydrofoil. As the flow passes the leading edge it continues to flow around the profile where parameters like maximum thickness and curvature affect the flow kinematics. These two parameters increase flow velocity on the suction side in comparison to the pressure side of the blade's profile. An increase in local flow velocity decreases the local pressure in the boundary layer, which in turn increases the

Journal of Fluids Engineering. Received October 11, 2017;
Accepted manuscript posted November 15, 2018. doi:10.1115/1.4041985

probability of boundary layer separation and cavitation inception [9]. From the turbine's velocity triangles, the relative velocity along the blade chord increases on both sides and is higher at the trailing edge of the blade [12]. Alternatively, the actual velocity within the runner decreases and enables energy conversion. Any discussion, therefore, on cavitation properties must be based on the differences between the actual velocities that exist between blade designs. In addition, a comparison of the pressure difference between designs along the entire blade chord is needed.

After determining the most important parameters of the blade profile, the following parameters of blade profile were modified: the leading edge shape radius, the position of maximum thickness and profile curvature. The leading-edge shape radius was increased and the position of both maximum thickness and curvature were shifted towards the leading edge. The new turbine blade profile was named the modified turbine blade profile. Characteristics of both turbine blade profiles are given in Table 1. The modified blade design relative to the unmodified design produces a higher pressure and as a result a lower absolute velocity in a broad region from the point of maximum thickness to the trailing edge. Therefore, the modified blade has, from the viewpoint of cavitation inception, an advantage in this region relative to the unmodified design. However, the unmodified blade has an advantage in the initial chord section, i.e., from the leading edge towards the point of maximum thickness but the area of this region is small in comparison. This is valid only for the best efficiency point but turbines do not always operate under optimal conditions. When operating away from optimal conditions the large radius of the leading edge, influenced by the shift in the max

Journal of Fluids Engineering. Received October 11, 2017;
Accepted manuscript posted November 15, 2018. doi:10.1115/1.4041985

thickness of modified blade towards leading edge, helps mitigate unfavorable flow conditions and flow separation either near or directly after the leading edge.

Figure 3 shows both the modified and unmodified turbine blade profiles. As discussed above (Figure 1), both the modified and unmodified turbine blade profile locations correspond to unmodified Kaplan runner blades at 95 % of the radius *R*. The modified profile was applied to the whole span of the runner blade.

The unmodified and modified blade runner profiles (Figure 3) were designed as 2D profiles in a x-y Cartesian coordinate system. To obtain a spatial shape of the modified 3D turbine blade the procedure was now reversed. After designing the modified hydrofoil, based on a 95 % of nominal Kaplan runner radius *R*, the next step was to design the whole Kaplan runner blade shape incorporating the modified turbine blade profiles. The dimensional characteristics of the unmodified and modified Kaplan runner blades are shown in Table 2. The unmodified and modified runners were manufactured using standard materials using the same technology and both received the same surface finish by grinding and polishing.

3. MATERIAL AND METHODS

3.1 Measuring turbine characteristics

Experiments were performed on a test rig designed for performance testing of low-head axial and bulb turbines (Figure 4) in Turboinstitute (Ljubljana, Slovenia). The

Journal of Fluids Engineering. Received October 11, 2017;
Accepted manuscript posted November 15, 2018. doi:10.1115/1.4041985

test rig is also used for turbine model performance testing according to the IEC 60193 standard [13], for research and development of new turbine runners and performing model witness and acceptance tests. The proper selection of measurement methods and equipment ensures high accuracy and repeatability. In addition, to comply with IEC 60193 standard [13] all measurements were automated.

The test rig's nominal runner diameter is 350 mm and the flow is provided by two water supply pumps with 110 kW total power each and frequency regulation. The maximum pump head is >30 m and the maximum flow rate is around 1.1 m^3/s.

Flow was measured using an electromagnetic flow-meter with a nominal diameter of DN400 and a nominal accuracy of ± 0.15% at 0.1 to 1m^3/s (normal operation regimes). Flow-meter frequency signal outputs were processed using counter-timer modules with a nominal accuracy of ± 0.01 % during normal flow conditions [14 and 15]. Total specific energy consists of the sum of the static and dynamic part. The static part of the specific energy was measured with a differential manometer with an accuracy of ± 0.025 %. Two pairs of measuring taps on the model turbine inlet and two pairs on the outlet were used to measure pressure. The measurements were made in compliance with IEC 60193 standard [13]. The dynamic part was calculated from the average velocities across both cross-sections of the measuring planes on the turbine inlet and outlet [14 and 15]. Net positive suction energy was measured on the low-pressure side of the turbine at the suction collector of the turbine outlet cross section [14 and 15]. Rotational speed was measured using an electromagnetic incremental non-contact sensor with pulse output connected to a counter-timer input module with a nominal accuracy of ±0.01 %. The rotational speed sensor was mounted on the top of the brake generator. The frequency signal from the counter input was further averaged and converted to rpm using the measuring software [14 and 15]. Shaft torque was measured using a high precision digital rotating transducer (nominal accuracy: 0.01%), mounted on a horizontal shaft. The friction torque was estimated from the rotational speed and axial force. The motor generator on the turbine shaft maximum power was 182 kW, maximum rotational frequency was 1480/min and maximum torque was 1170 Nm.

Water temperature was measured with a Pt 100 sensor built into the pipe wall. The water and air temperature was then used to calculate water and air density according to IEC 60193 [13].

Both the unmodified and modified turbine runners were tested under equivalent operating regimes to investigate the influence of blade shape on cavitation inception, cavitation development, and turbine efficiency. Acceptance tests for assessing cavitation occurrence in Kaplan turbines are usually performed at blade angles β from 18 ° to 32 °, depending on turbine properties and on the operating environment. Operating points were, for the sake of comparison, set according to the hill diagram of the unmodified turbine runner (Figure 5). Measurements were performed at six operating points at a blade angle of β = 25 °. This value of angle β was determined by the chord line and blade orientation (Figure 6) and set using an angle template. Only operating points of equal energy number ψ for both modified and unmodified runners were selected. This was done to show the influence of different turbine heads on cavitation occurrence, because at low energy numbers cavitation phenomena is more intense.

Energy numbers ψ were calculated according to IEC 60193 [13]

$$\psi = \frac{2 \cdot E}{\pi^2 \cdot N^2 \cdot D^2} \quad . \tag{1}$$

In Equation 1 E [J/kg] is the specific energy of the turbine and defined as the difference between the total specific energy of the turbine inlet and the outlet. N [min^{-1}] is turbine rotational speed and D [m] is nominal diameter of turbine which is for the case of Kaplan turbine diameter of the discharge ring.

According to the hill diagram (Figure 5) and ψ, two additional parameters were equal for both runners, turbine rotational speed N (1000 min^{-1}) and the guide vane opening coefficient A_0 [14 and 15]

$$A_0 = \frac{a_{\mathrm{v}} \cdot z}{D_{\mathrm{v}}} \quad . \tag{2}$$

In the equation (2) a_{v} [mm] is the minimal distance between two guide vanes, z [/] is the number of guide vanes and D_{v} [mm] is the wicket gate pitch diameter. Runner tip clearances and clearences between the passage and guide vanes are of major importance in achieving the efficiency of model turbine runners. In this project the well-established procedures of the Turboinstitute's (Ljubljana, Slovenia) model runner manufacturing practices were followed, enabling measurements of efficiency of around 0.15%. In general, runner tip clearances were from 0.1 to 0.2 mm and the clearences on the guide vanes were below 0.05 mm. These values, however, depend on the angle of the runner and on the apparatus clearences, which is the average value of the upper or lower apparatus rings. In this case, the set angle of both runners was 25° and was within

Journal of Fluids Engineering. Received October 11, 2017;
Accepted manuscript posted November 15, 2018. doi:10.1115/1.4041985

the interval of the runner tip clearances and as such valid for the entire length of the blade of the tip.

Since the test rig is of a closed type, to keep the ψ at the selected value, the two main feeding pumps were regulated by varying their rotational speed. The volume flow rate Q [m^3/s] is a dependent variable and was in the non-dimensional form widely used in acceptance tests represented as flow rate number φ [13].

$$\varphi = \frac{Q}{\pi^2/4 \cdot N \cdot D^3} \quad . \tag{3}$$

In order to obtain the model turbine cavitation curve characteristics σ - η_T (Figures 7 to 12) the cavitation number σ and turbine hydraulic efficiency η_T were also evaluated. High cavitation numbers correspond to low probability for cavitation and low cavitation numbers correspond to high probability. Cavitation number σ is calculated according to IEC 60193 as follows [13]:

$$\sigma = \frac{NPSE}{E} = \frac{\frac{p_{\mathrm{abs2}} - p_{\mathrm{va}}}{\rho_2} + \frac{v_2^2}{2} - g \cdot (z_{\mathrm{r}} - z_2)}{E} \quad , \tag{4}$$

where $NPSE$ is the Net Positive Suction Energy [J/kg], z_r [m] is the reference constant level and p_{va} [N/m^2] is the water evaporation pressure. Absolute pressure, water velocity and the water level at the draft tube outlet section are marked as p_{abs2}, v_2 and constant z_2. Water evaporation pressure was determined on site with an established Equation (5)

Journal of Fluids Engineering. Received October 11, 2017;
Accepted manuscript posted November 15, 2018. doi:10.1115/1.4041985

$$p_{va} = 10^{2,7862+0,0312 \cdot T_w - 0,000104 \cdot T_w^2}, \qquad (5)$$

where T_w stand s for water temperature. The Equation (5) gives a maximum deviation of 0.2%, which has a small influence on the measurements and for this reason the above-defined equation is acceptable [14 and 15].

Efficiency η_T was calculated as

$$\eta_T = \frac{P_M}{\rho \cdot E \cdot Q} \quad . \qquad (6)$$

In Equation (6) P_M is mechanical power [kW] generated by the turbine, ρ is water density [kg/m^3] and Q is the volume flow rate [m^3/s].

For each cavitation curve, the first cavitating point is always measured at ambient pressure p_0 while for subsequent cavitating points the rotational speed of the vacuum pump is increased and the suction pressure or suction head (H_s) decreases to reach the next operating point. The cavitation curve ends when the suction pump pressure can no longer be decreased due to leakages in the test rig. To construct the cavitation curves (Figures 7 to 12) the turbine was operated in an interval of cavitation numbers from incipient cavitation σ_i (cavitation number where cavitation may be first visually observed), to σ_0 (measurable influence on turbine efficiency) and finally to σ_{-1} (turbine efficiency drops for more than 1%). σ_{pl} is the cavitation number of the hydropower plant. All types of cavitation on the blade of the Kaplan turbine were achieved during cavitation tests and included the following: incipient cavitation, partial

Journal of Fluids Engineering. Received October 11, 2017;
Accepted manuscript posted November 15, 2018. doi:10.1115/1.4041985

cavitation such as sheet cavitation, intermittent cavitation, cavitation clouds and supercavitation [6].

3.2 Experimental setup for flow visualization

Flow visualization measurements were performed on the same test rig with minor modifications of the flow tract. These modifications were made in order to observe cavitation phenomena on the suction side of the runner blades. For this purpose, the draft tube cone was made from polished Plexiglas. The experimental setup is shown in Figure 4.

A Fastec Hispec4 camera was used with a Nikkor 50 mm 1:1.2 lens to capture the cavitation phenomena. The camera was triggered by an inductive sensor trigger on the Kaplan turbine shaft. One image per shaft rotation was acquired to record images of cavitation on the same blade. Images were recorded in 8-bit BMP black and white format and with a resolution of 688x1570 using HiSpec software from Fastec. Shutter speed was set to 150 µs. For each operation point 1982 frames over a period of 1.86 seconds were recorded. A high intensity continuous LED provided illumination and was located near the camera on the suction side of the blade such that no reflections were visible in the recorded images.

3.3 Image analysis

Journal of Fluids Engineering. Received October 11, 2017;
Accepted manuscript posted November 15, 2018. doi:10.1115/1.4041985

Cavitation structures, which emerged on the blades of the Kaplan turbines, when illuminated, were recorded in a sequence of greyscale images. The cavitation structures appear as regions with increased grey level intensity, creating structures in time and space [3].

With subsequent digitalization of grey level intensities within the observed regions of interest or windows, simultaneous scalar time series were obtained. An assumption is made that the intensity of light in the image is proportional to the amount and intensity of the void fraction (vapor phase), which is in turn proportional to the amount of cavitation structures in the observation window [16]. This assumption is valid for low intensities of cavitation, low void fractions and proportional ratios between the vapor phase volume and grey level. In addition, the assumed proportionality between void fraction and intensity of light is justified since it is used for comparative and qualitative analysis purposes only.

The local grey level intensity $E(i,j,t)$ was measured with 256 grey levels (8-bit camera resolution) of greyscale intensity from black (intensity = 0) to white (intensity = 255). The time series for the averaged grey level intensities were calculated for each observation window. The standard deviation was calculated according to the following equation:

$$S(i,j) = \sqrt{\frac{1}{T}\sum_{t=1}^{T}[E(i,j,t) - \langle E(i,j)\rangle]^2} \quad . \qquad (7)$$

Journal of Fluids Engineering. Received October 11, 2017;
Accepted manuscript posted November 15, 2018. doi:10.1115/1.4041985

where $\langle E(i,j)\rangle$ is time averaged, spatially averaged, grey level intensity that is proportional to the average void fraction of the cavitation structure's intensity, i.e.,

$$\langle E(i,j)\rangle = \frac{1}{T}\sum_{t=1}^{T} E(i,j,t) \quad . \tag{8}$$

The time interval *t* in Equations 7 and 8 is derived from the frequency of image acquisition and the number of acquired images. The analysis was performed using the Dynascan [17] software package.

4. RESULTS AND DISCUSSION

Two Kaplan turbine runners with different blade designs were tested. First, the performance of the two Kaplan runners was analyzed as a function of cavitation number (section 4.1). The goal was to demonstrate that the modified blades increase turbine efficiency and decrease cavitation occurrence. The focus was then placed on visualizing cavitation phenomena including the cavitation structures and their location on the suction side of the runner blade (section 4.2).

4.1 Turbine performance

Turbine performance was measured for the unmodified and modified runner design and is represented as a cavitation curve for every operating point from the hill diagram (Figure 5). The focus was on the drop in hydraulic efficiency as a function of the cavitation number (Figures 7 to 12) in accordance with IEC 60193 standard [13]. Measurements on the modified blade were done for six pressure numbers at a blade angle of 25° in order to validate the new design (Figure 6). Because both runners are not exactly the same, their hill diagrams cannot be compared. Figure 3 shows how the blade leading and trailing edges slightly changed, albeit the turbine blade angle was maintained.

There are, however, convincing evidences for points ψ_4=0.1513 and ψ_5=0.2062. Here the lines of constant efficiency on the hill diagram are almost parallel to the φ axis and the shift in flow number is unlikely to produce any significant improvement in efficiency unless the blade design is improved.

Figures 7 to 12 show cavitation curves for both runners. The overall hydraulic efficiency of the modified runner is at least 1% higher. In the case of the modified runner, incipient cavitation σ_i starts much later at lower cavitation numbers than on the unmodified runner where incipient cavitation starts earlier at higher cavitation numbers. With regards to turbine operation, the cavitation number σ_0 is an important variable, where cavitation occurrence starts to affect turbine performance and efficiency. The modified runner is less susceptible to cavitation occurrence and its development. Therefore, the modified runner can withstand operating points with lower suction pressure and higher discharges before any decrease in efficiency can be measured.

The cavitation number σ_{-1} designates those operating conditions, where the turbine efficiency drops by more than 1 %. At a cavitation number of σ_{-1} the large

Journal of Fluids Engineering. Received October 11, 2017;
Accepted manuscript posted November 15, 2018. doi:10.1115/1.4041985

cavitation structures start to reduce the water passage cross section and discharge through the runner. Again, from the results it is clear that the modified runner has better characteristics than the unmodified design. The efficiency of the modified runner drops at lower cavitation numbers. In addition, the modified runner can operate at higher suction heads and is able to achieve a higher efficiency over a broader interval of suction heads.

The cavitation curves (Figures 7 to 12) include images of sample cavitation structures for each cavitation point on the suction side of runner blades. For every cavitation curve and corresponding ψ the images of the modified runner show less pronounced cavitation structures, while the unmodified blade shows more pronounced cavitation structures even at higher cavitation numbers. Cavitation along the unmodified runner occurs in several regions, among them on the tip edge of the blade and also at the root of the blade, which is evidence that the blade shape is suboptimal [6].

A special case is shown for ψ_4. At this operating point the parameters σ_0 and σ_{-1} from the acceptance measurement standard [13] could not be set due to the influence of cavitation on the turbine's characteristics and limitations of the test rig.

4.2 Analysis of the cavitation structures

Journal of Fluids Engineering. Received October 11, 2017;
Accepted manuscript posted November 15, 2018. doi:10.1115/1.4041985

Cavitation structures (void fraction) were analyzed using computer aided visualization, which shows the results of a series of image analyses. Below, the topology of the cavitation structures, their position and intensity are discussed.

The cavitation number σ_i, denotes cavitation inception. For all operating points, incipient cavitation is present on the edge of the blade tip, where fluid velocity is the highest. Here, a pressure drop occurs in the gap between the pressure and suction side of the blade.

Incipient cavitation is at first present as attached cavitation on the junction of leading and tip edge of the blade. With a further decrease in the cavitation number, the attached cavitation becomes enlarged and covers the entire tip edge including the tip of the leading edge. Flow separation that occurs in the boundary layer is present close to the stagnation point. Closer to the blade re-entrant flow is formed and a vortex wake can be visually identified. The first cavitation clouds are formed due to quasi periodic pressure fluctuations, at approximately one-third of the blade chord length. The location of completion (termination) of the cavitation structures moves towards the trailing edge of the blade, which from the viewpoint of cavitation damage is undesirable. A further decrease in the pressure causes the cavitation to extend to the entire region between the hub and the blade tip. Here, intense cavitation clouds are formed, which significantly decrease hydraulic turbine efficiency. At the same time cavitation on the tip edge slowly changes into supercavitation, while an excited wake forms extending out from the passage of previous blade. This causes a sharp decrease in volume flow rate and efficiency.

Journal of Fluids Engineering. Received October 11, 2017;
Accepted manuscript posted November 15, 2018. doi:10.1115/1.4041985

The topologies associated with the cavitation structures were analyzed using computer aided visualization (see subsections 3.2 and 3.3). The operating and cavitation points were selected according to the corresponding ψ to show the influence of the hydraulic turbine efficiency η. Cavitation numbers σ (for the selected ψ) were different for both designs on purpose to allow similar amount of cavitation and thus comparison. In the following results, the distributions of time-averaged local image intensity $\langle E(i,j) \rangle$ and its standard deviation $S(i,j)$ are shown. The former shows the cavitation zone around the runner blade, while the latter represents the strength/aggressiveness of fluctuation of cavitation.

For ψ_1 (Figure 13), cavitation numbers of σ = 0.9 (modified runner) and σ = 1.2 (unmodified runner) were compared. Here, a noticeable difference in the cavitation structures is present. The cavitation around the modified runner at σ = 0.9 is, despite having a lower cavitation number, less pronounced than the original runner operating at σ = 1.2. This means that when using same cavitation number σ, cavitation would be even more developed in the case of the original runner design. For the modified runner, cavitation along the edge of the tip remains attached and localized, while for the unmodified runner cavitation clouds appear from the upper part from the leading edge until the trailing edge. This is of concern during extended operation, since it can lead to cavitation damage at the tip of the runner blades. Cavitation clouds can also develop at the blade fillet. This should be avoided from the viewpoint of high efficiency, as this type of cavitation decreases turbine efficiency η.

A similar behavior is observed for ψ_2. Here cavitation numbers of σ = 1.2 (modified) and σ = 1.5 (unmodified) were compared (Figure 14). Because of the lower energy number ψ, cavitation is present already at higher cavitation numbers σ. At this operating point, cavitation developed on the unmodified runner is mainly found in two regions: at the outer edge as boundary layer shedding and behind the leading edge as flow separation. At approximately one-third of the blade chord, flow transition from excited cavitation to developed cavitation occurs. In the case of the unmodified runner design flow separation is more intense, especially near the hub, where the influence on η is significant. For both runner designs cavitation cloud vortices are formed, collapsing near the remaining third of the blade chord near the blade trailing edge. The collapse of cavitation clouds at this point is dangerous, because it is located at approximately 2/3 of the blade chord length. In this region, the collapse of the cavitation clouds are most problematic for cavitation erosion [18] due to the intensity of the process. For the unmodified runner design, the shedding of the boundary layer is initiated after the leading edge of the blade. The formation of intense cavitation clouds between the blade and the hub is also undesirable and leads to a decrease in efficiency η compared with modified runner. Formation of cavitation here further enhances local flow instabilities due to the suboptimal blade shape [6].

The situation for ψ_3 is shown in Figure 15. Here, cavitation numbers of σ = 1.3 (modified) and σ = 1.6 (unmodified) were compared. A large difference in the cavitation structures is observed between both runner designs. For the unmodified runner, cavitation at the tip of the blade prevails while mild cavitation is present near the blade

Journal of Fluids Engineering. Received October 11, 2017;
Accepted manuscript posted November 15, 2018. doi:10.1115/1.4041985

fillet. Cavitation clouds are formed only at the tip near the trailing edge. The cavitation structures greyscale intensity is lower at the modified runner. The unmodified runner exhibits fully developed cavitation structures in three regions, on the blade edge, at the leading edge and at the blade fillet. The development of cavitation on the leading edge confirms sub-optimal shape of leading edge of the unmodified blade.

For ψ_4 σ = 2.0 (modified) and σ = 2.4 (unmodified) were compared (Figure 16). At this energy number high intensity cavitation occurs with a large difference in cavitation intensity between the cavitation structures observed for different runner designs. For the unmodified runner, intense cavitation is present at the tip edge due to the influence of the pressure field of the adjacent blades. High fluctuations in the cavitation clouds are present at the tip of the blade. In addition, intense cavitation in the form of cavitation clouds occurs in the region of the blade fillet, leading to a noticeable decrease in η, the unmodified runner performs worse than the modified runner. In the case of the modified runner, a thin band of attached cavitation and limited flow separation is observed. At the trailing edge of the blade, the formation of small cavitation clouds is also observed.

At ψ_5 (Figure 17) cavitation numbers of σ = 1.6 (modified) and σ = 1.9 (unmodified) were compared. The results are similar to the previous operating point. Similar cavitation structures are formed, however at a much lower σ. The interpretation of the cavitation properties is similar as in the previous operating point.

At ψ_6 (Figure 18), σ = 0.70 (modified) and σ = 1.00 (unmodified) were compared. For both runners cavitation is present at the blade fillet and at the tip edge. At the tip

Journal of Fluids Engineering. Received October 11, 2017;
Accepted manuscript posted November 15, 2018. doi:10.1115/1.4041985

edge, however, cavitation on the modified runner ends at approximately halfway along the chord length. On the unmodified runner's tip edge cavitation extends across the entire chord length. Figure 18 shows intense cavitation clouds. The unmodified runner also exhibits sheet cavitation. Sheet cavitation causes the cavitation structures to appear on the entire suction side of the blade. For the modified runner, problems with illumination meant that the intensity of the standard deviation of the grey level was higher overall.

5 CONCLUSIONS

The purpose of this study was to determine the influence of Kaplan turbine blade shape on turbine efficiency and cavitation properties. Modifications of Kaplan turbine blades were performed. The unmodified blade profile was extracted at 95 % of radius of the blade. Hydrofoil shape was changed such the leading-edge shape radius was increased and the position of both maximum thickness and curvature were shifted towards the leading edge.

Measurements of the unmodified and modified Kaplan turbine characteristics were performed on the same low head test rig used for model turbine acceptance performance measurements. Measurements were carried out according to IEC 60193 standard [13] and the same rotational speed, energy number, guide vanes opening and blade angle were used, enabling the selection of operating points from the unmodified hill diagram in order to achieve a fair comparative analysis of both runners.

The pattern of cavitation development, under identical experimental conditions set with the aid of IEC 60193 standard [13] was similar for both runners and analysis of the cavitation curves for both runners showed that the modified runner was superior in all operating and cavitation points. Efficiency was also higher for 1 % and the modified runner was less sensitive to cavitation phenomena. In the case of the unmodified runner, incipient cavitation appears at higher cavitation numbers.

Computer aided visualization revealed substantial differences between the two runners, proving to be a valuable tool for cavitation research in hydraulic machinery [19]. In the case of the modified runner cavitation structures are less intense, and appear only in limited areas. Modified runner also exhibits improved cavitation and hydraulic properties. In a real hydropower plant, the modified runner would likely lead to increased electrical energy output, a wider operating area according to hill diagram and prolonged operating life.

6 ACKNOWLEDGEMENT

The authors gratefully acknowledge the financial support from Slovenian research agency (grant P2-0401) and support of Turboinstitute (KOLEKTOR TURBOINŠTITUT d.o.o., Rovšnikova 7, 1210 Ljubljana, Slovenia).

Journal of Fluids Engineering. Received October 11, 2017;
Accepted manuscript posted November 15, 2018. doi:10.1115/1.4041985

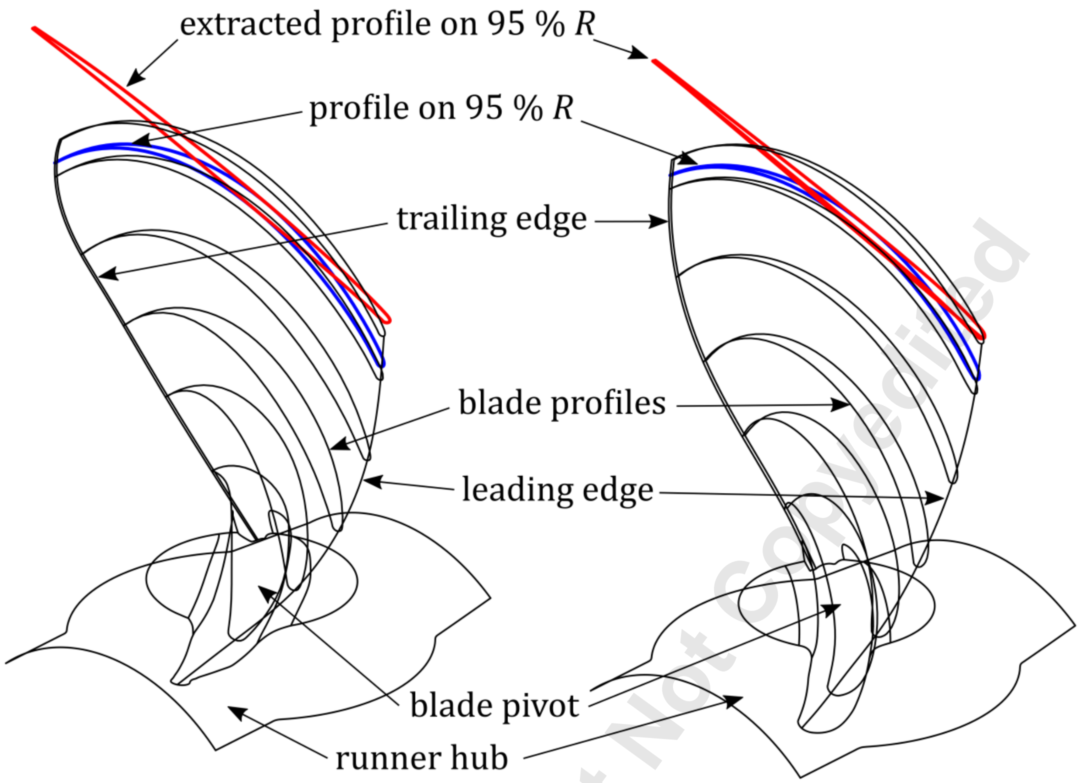

Figure 1: Location of extracted turbine blade profile on Kaplan runner blade, left: unmodified shape and right: modified shape.

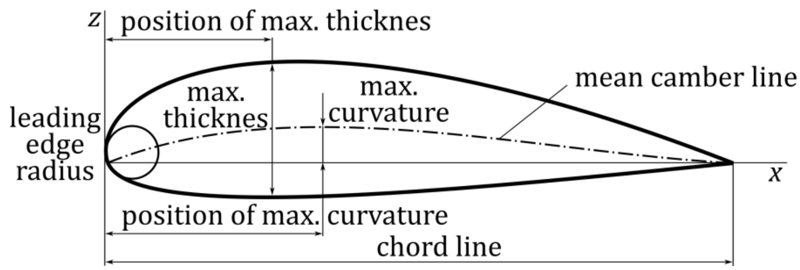

Figure 2: Most important parameters that set characteristics of turbine blade profiles

Journal of Fluids Engineering. Received October 11, 2017;
Accepted manuscript posted November 15, 2018. doi:10.1115/1.4041985

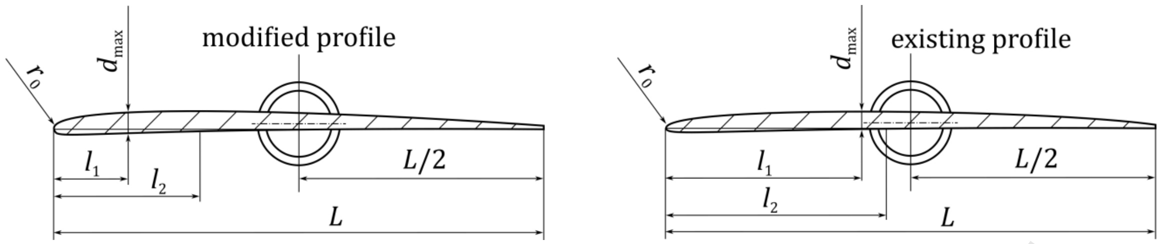

Figure 3: The difference in shape of both turbine blade profiles

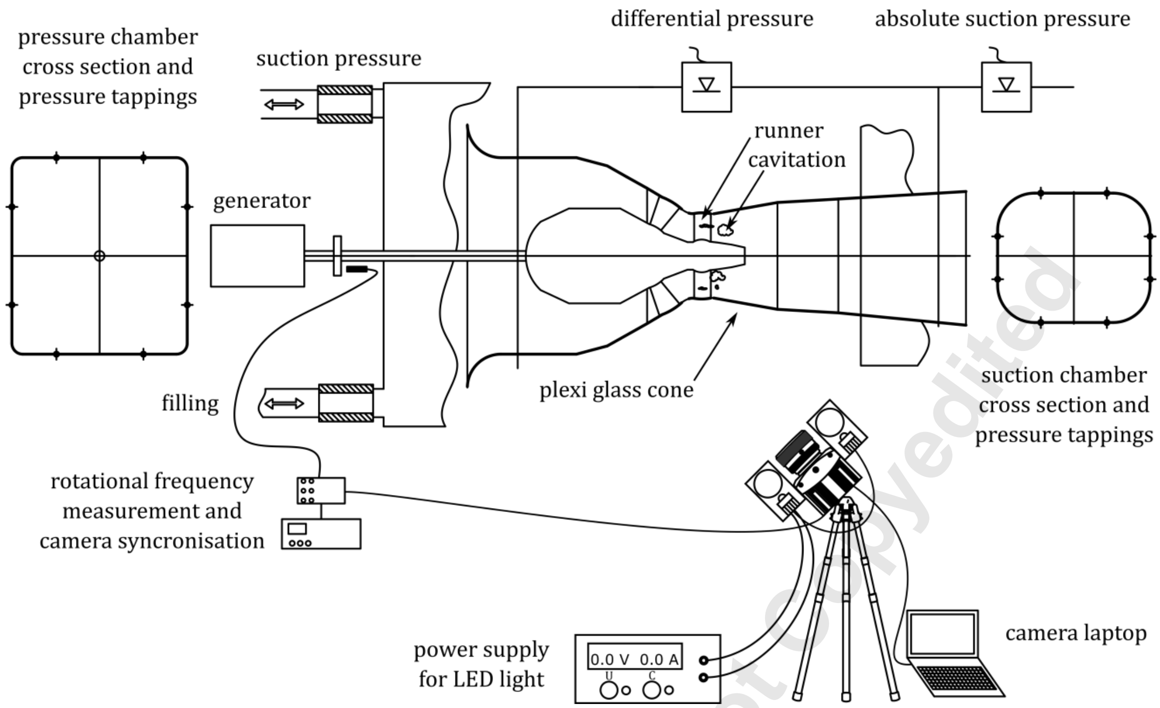

Figure 4: Experimental setup

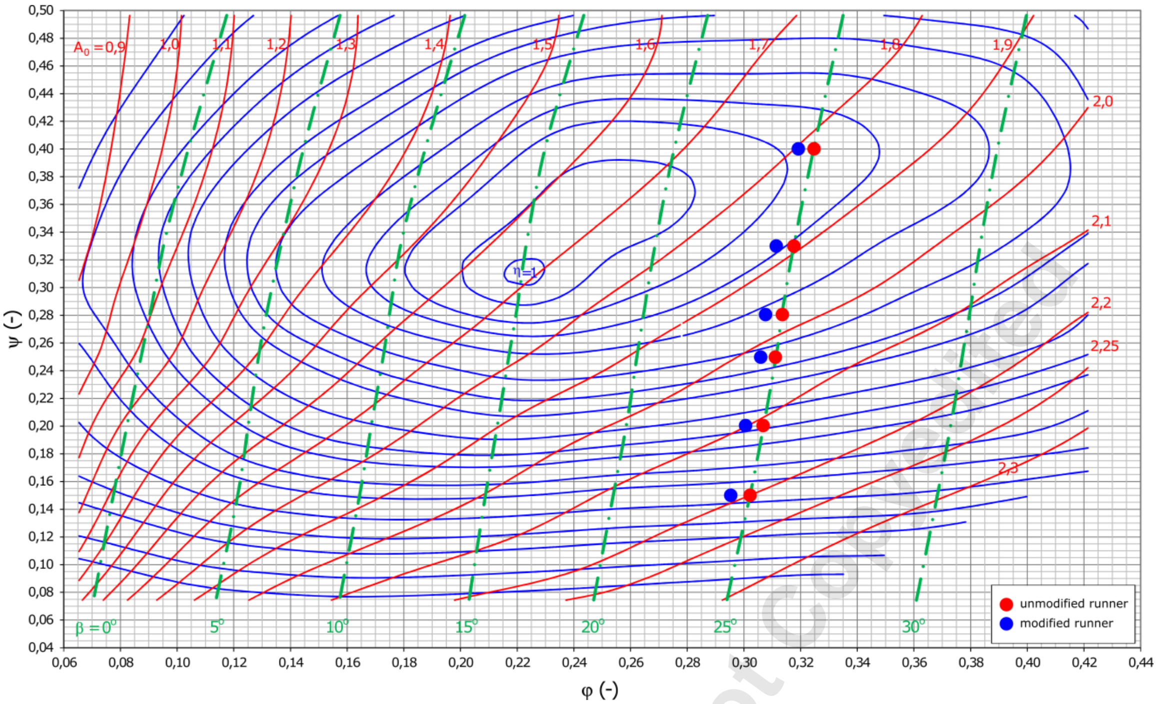

Figure 5: Original Kaplan turbine hill diagram with 6 selected ψ at blade angle β = 25 °

(courtesy of the Turboinstitute)

Journal of Fluids Engineering. Received October 11, 2017;
Accepted manuscript posted November 15, 2018. doi:10.1115/1.4041985

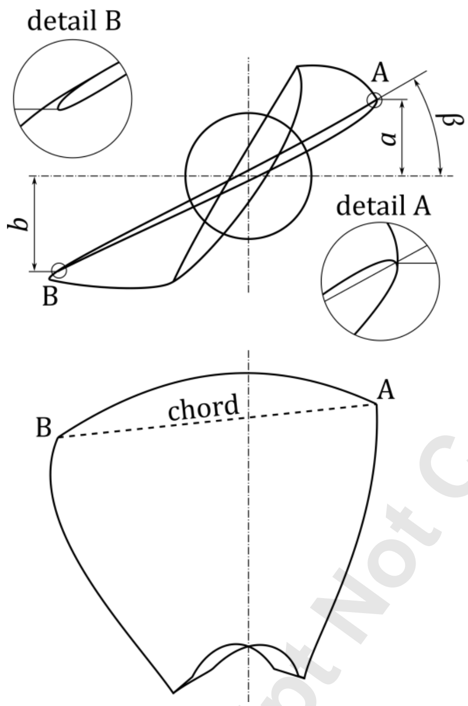

Figure 6: Runner blade angle β selection

Journal of Fluids Engineering. Received October 11, 2017;
Accepted manuscript posted November 15, 2018. doi:10.1115/1.4041985

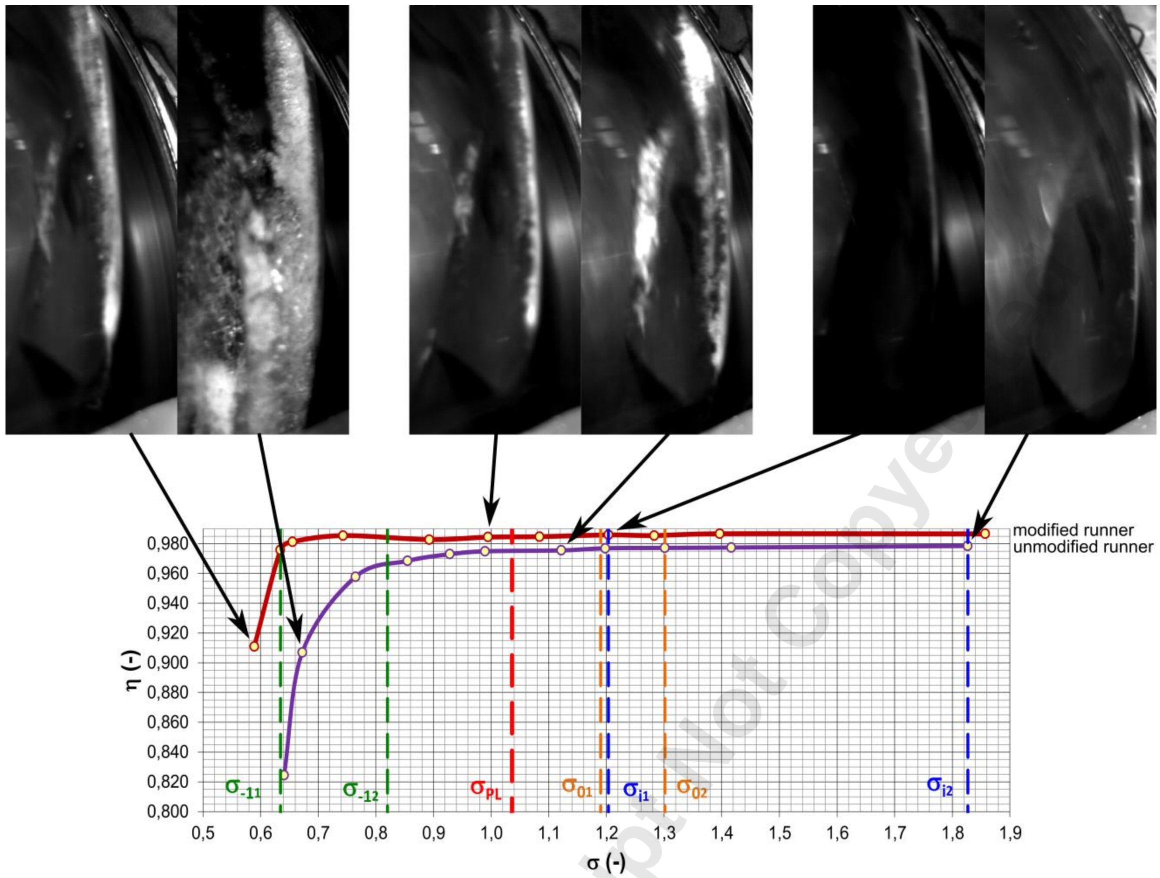

Figure 7: Cavitation curves for both runners at an ψ_1 = 0.3346

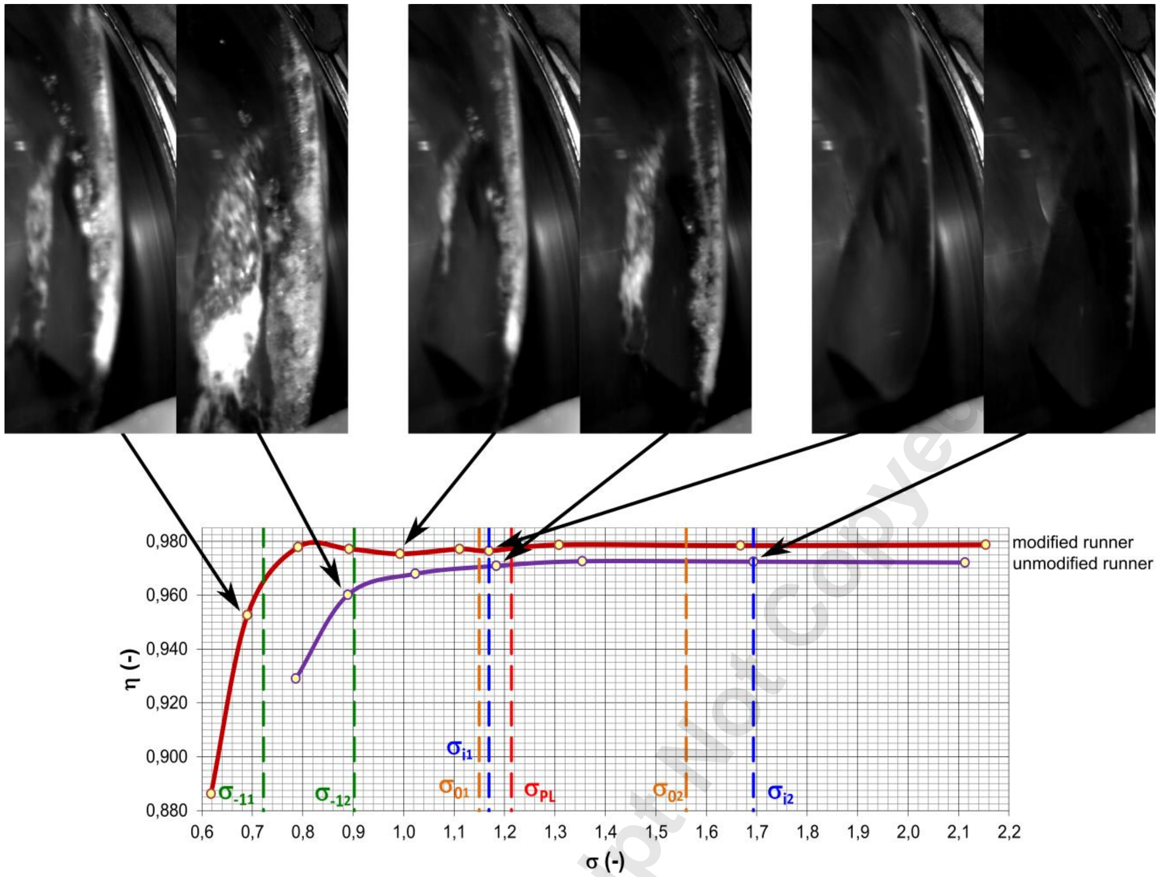

Figure 8: Cavitation curves for both runners at an ψ_2 = 0.2857

Journal of Fluids Engineering. Received October 11, 2017;
Accepted manuscript posted November 15, 2018. doi:10.1115/1.4041985

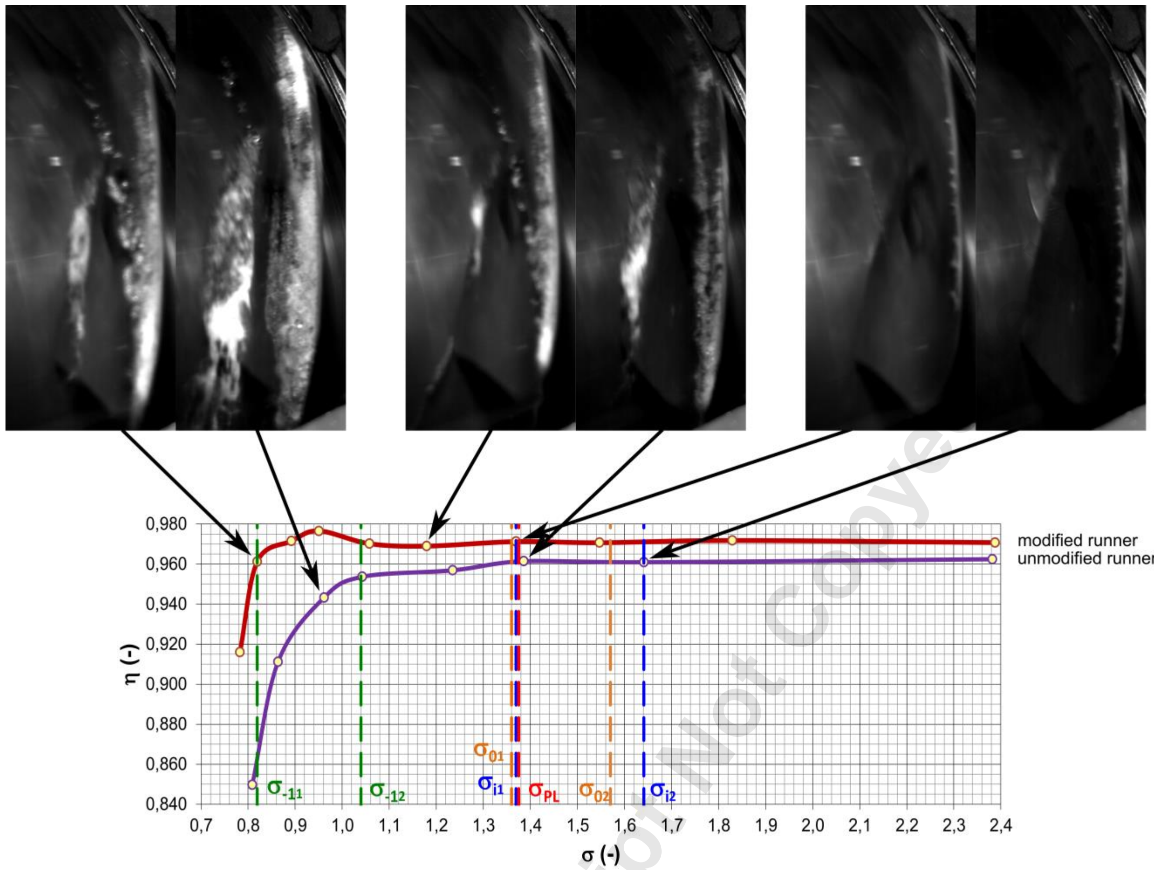

Figure 9: Cavitation curves for both runners at an ψ_3 = 0.2521

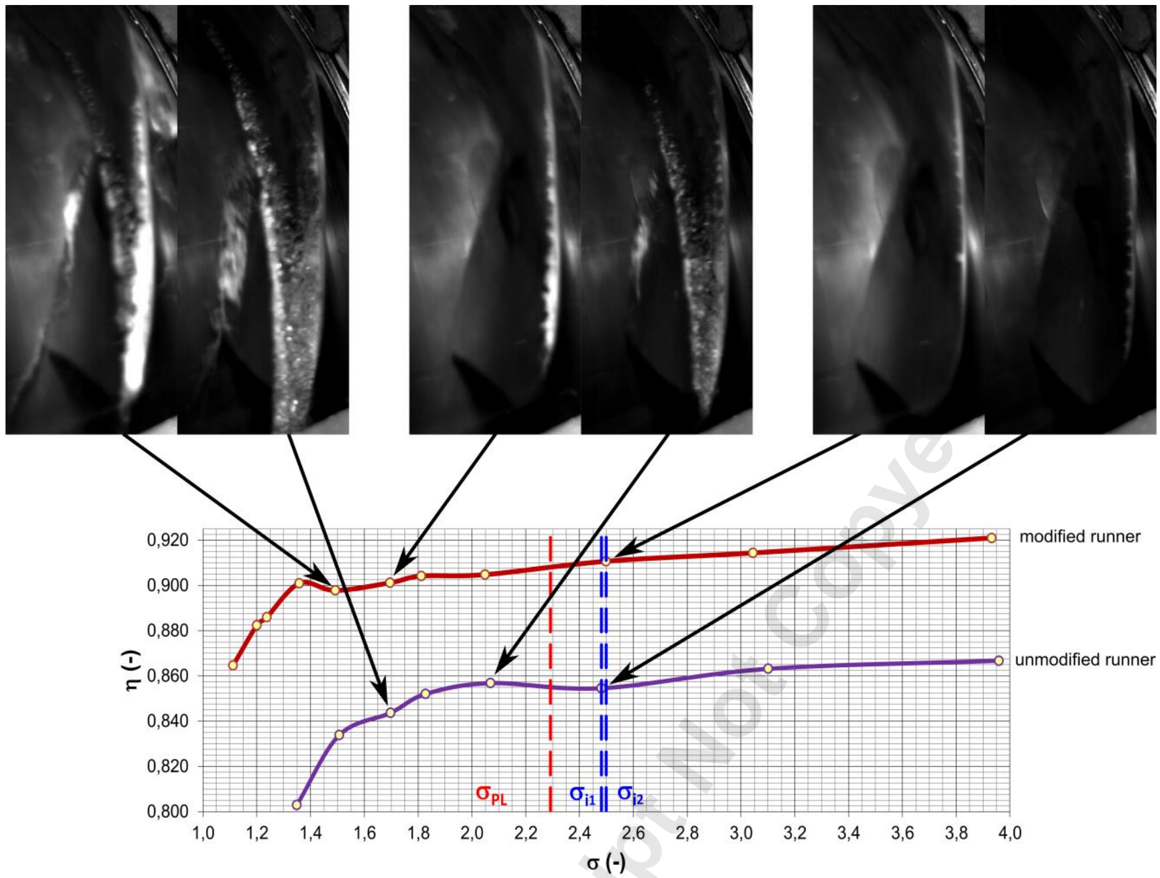

Figure 10: Cavitation curves for both runners at an ψ_4 = 0.1513

Journal of Fluids Engineering. Received October 11, 2017;
Accepted manuscript posted November 15, 2018. doi:10.1115/1.4041985

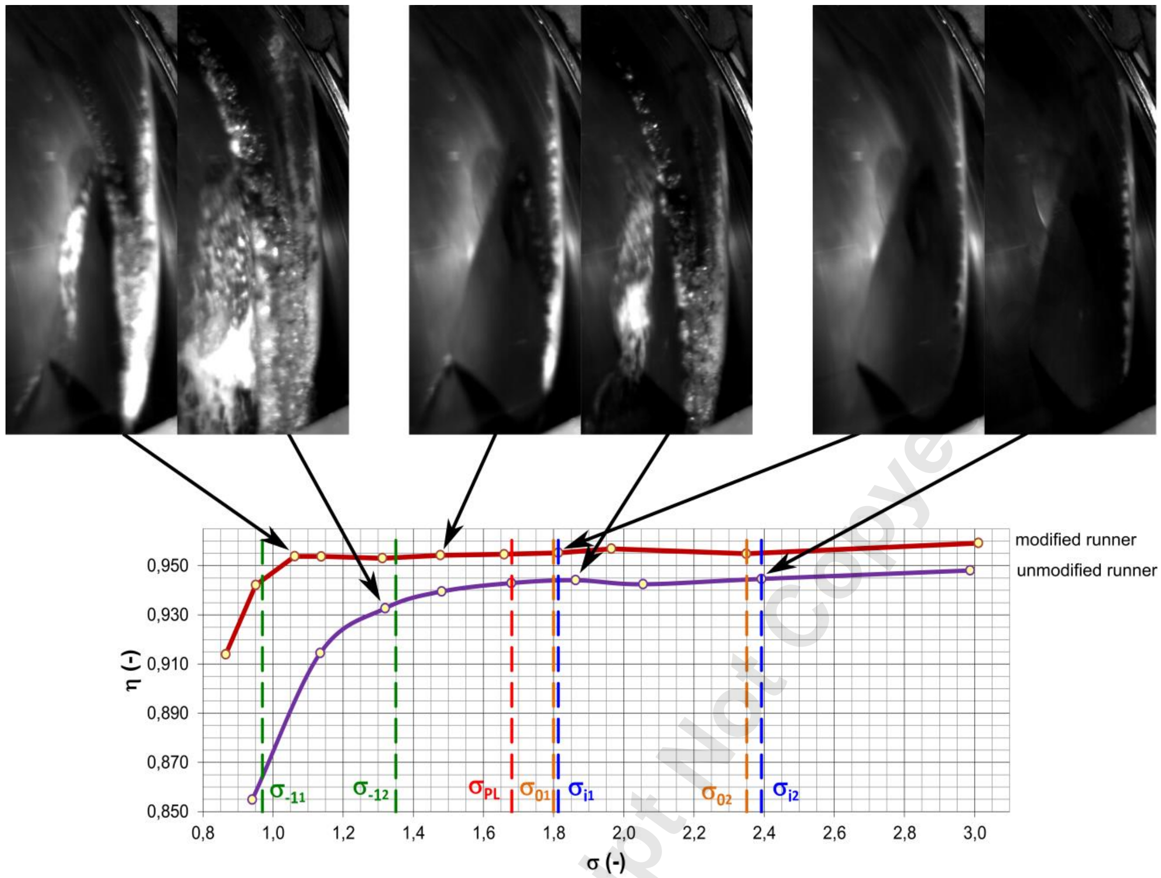

Figure 11: Cavitation curves for both runners at an ψ_5 = 0.2062

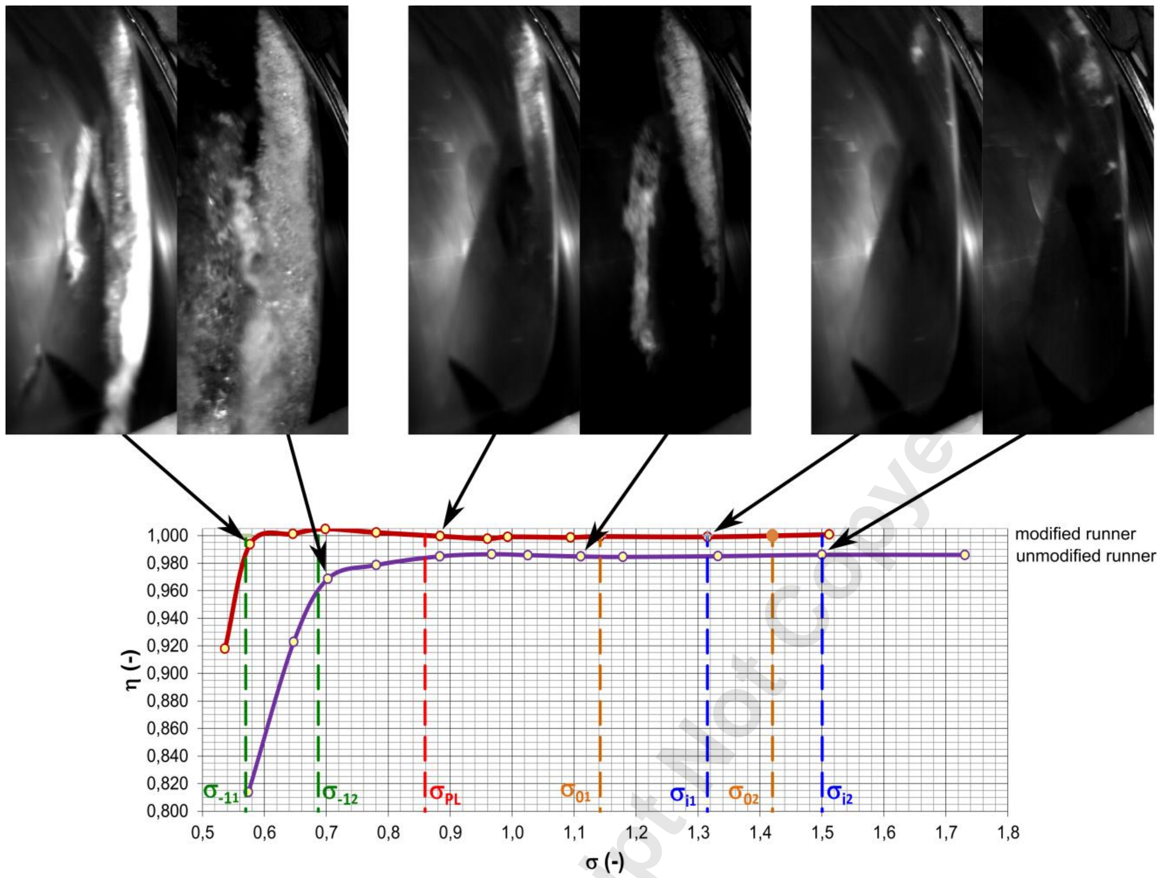

Figure 12: Cavitation curves for both runners at an ψ_6 = 0.4034

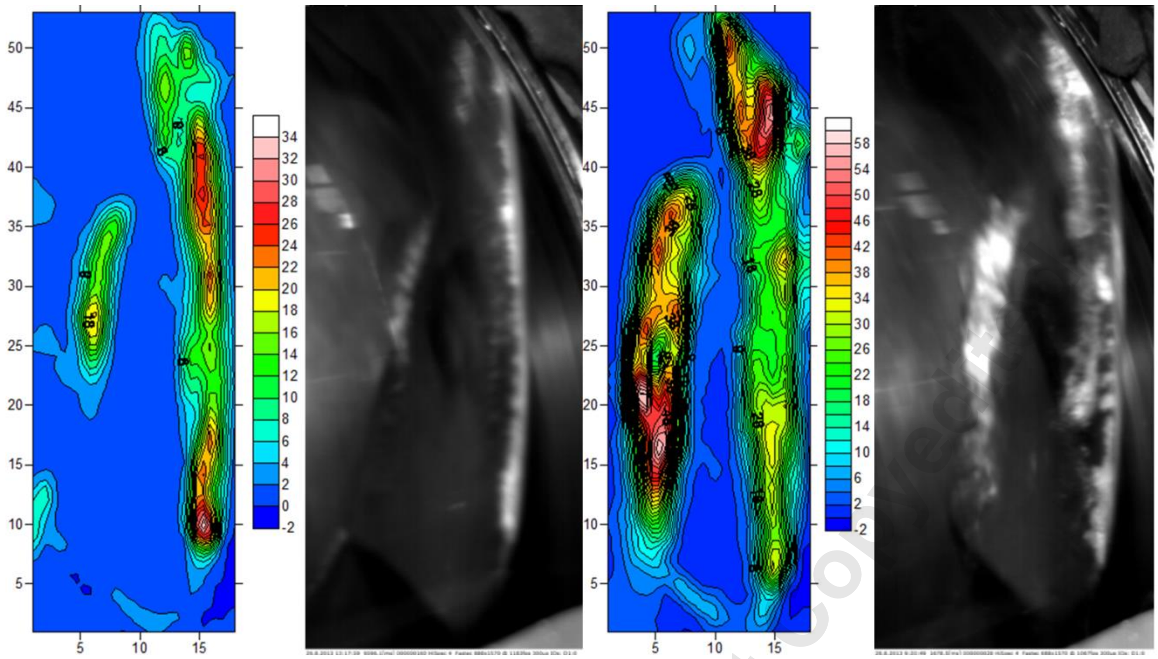

Figure 13: Standard deviation S and time averaged greyscale intensity $\langle A(k,t) \rangle$ *of cavitation structures for modified runner (left at σ = 0.9) and unmodified runner (right at σ = 1.2) at operating point (*ψ_1 *= 0.3346 and φ = 0.308)*

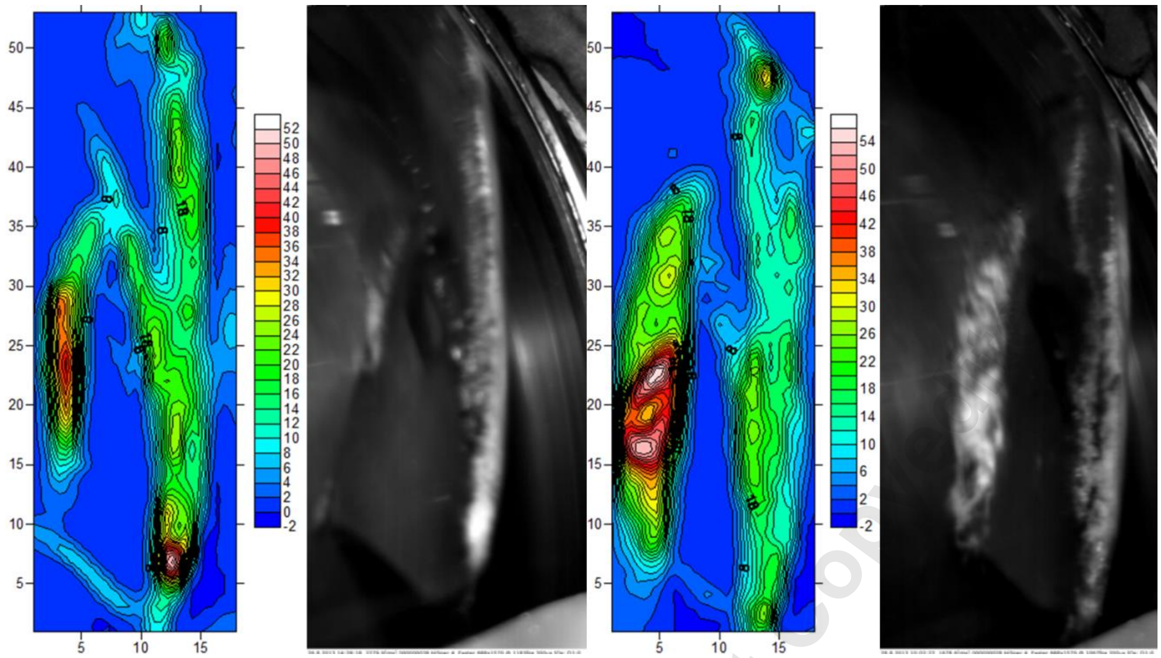

Figure 14: Standard deviation S and time averaged greyscale intensity $\langle \mathrm{A(k,t)} \rangle$ *of cavitation structures for modified runner (left at σ = 1.2) and unmodified runner (right at σ = 1.5) at operating point (*ψ_2 *= 0.2857 and φ = 0.31)*

Journal of Fluids Engineering. Received October 11, 2017;
Accepted manuscript posted November 15, 2018. doi:10.1115/1.4041985

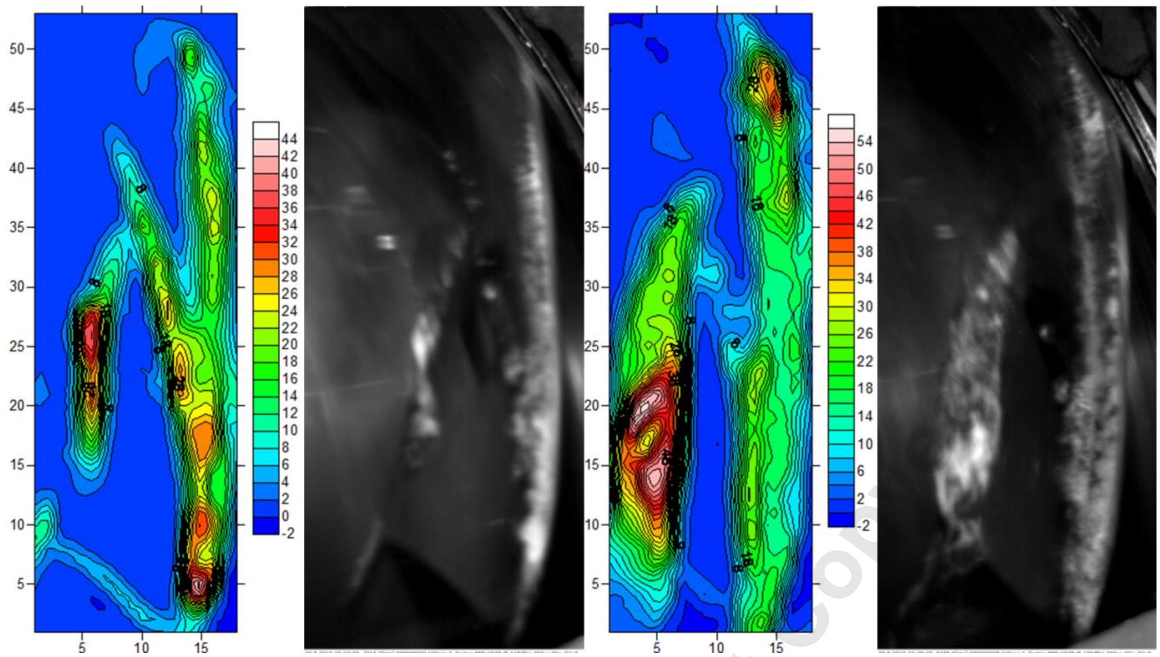

Figure 15: Standard deviation S and time averaged greyscale intensity $\langle A(k,t) \rangle$ *of cavitation structures for modified runner (left at σ = 1.3) and unmodified runner (right at σ = 1.6) at operating point (*ψ_3 *= 0.252 and φ = 0.318)*

Journal of Fluids Engineering. Received October 11, 2017;
Accepted manuscript posted November 15, 2018. doi:10.1115/1.4041985

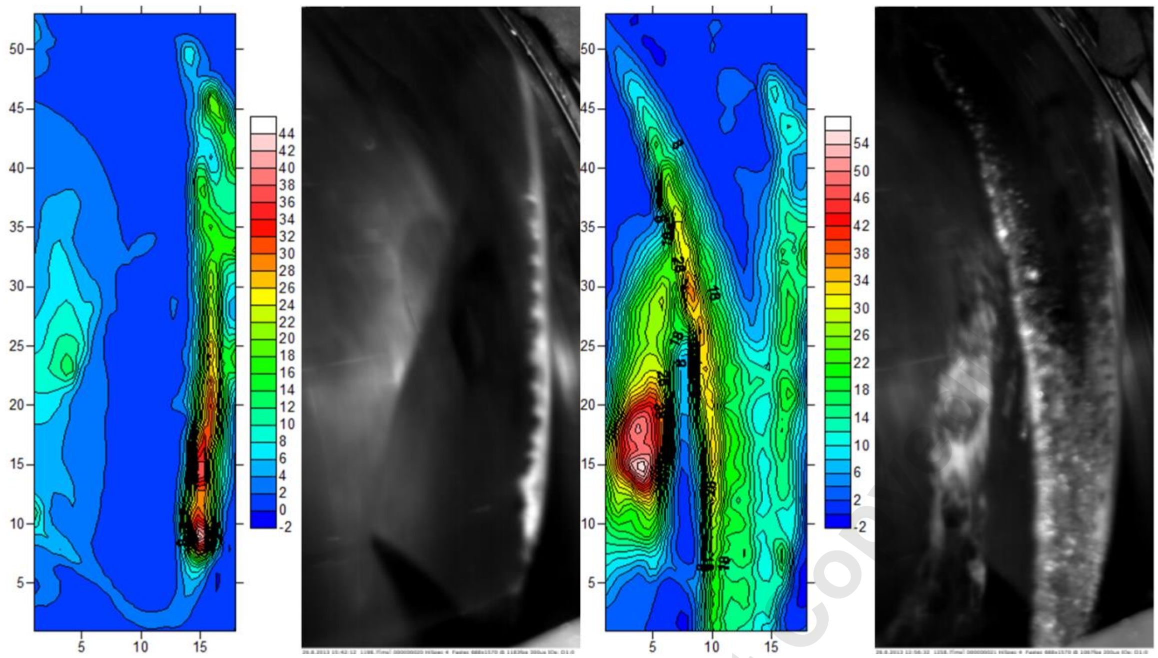

Figure 16: Standard deviation S and time averaged greyscale intensity $\langle \mathrm{A}(\mathrm{k},\mathrm{t}) \rangle$ *of cavitation structures for modified runner (left at σ = 2.0) and unmodified runner (right at σ = 2.4) at operating point (*ψ_4 *= 0.1513 and φ = 0.30)*

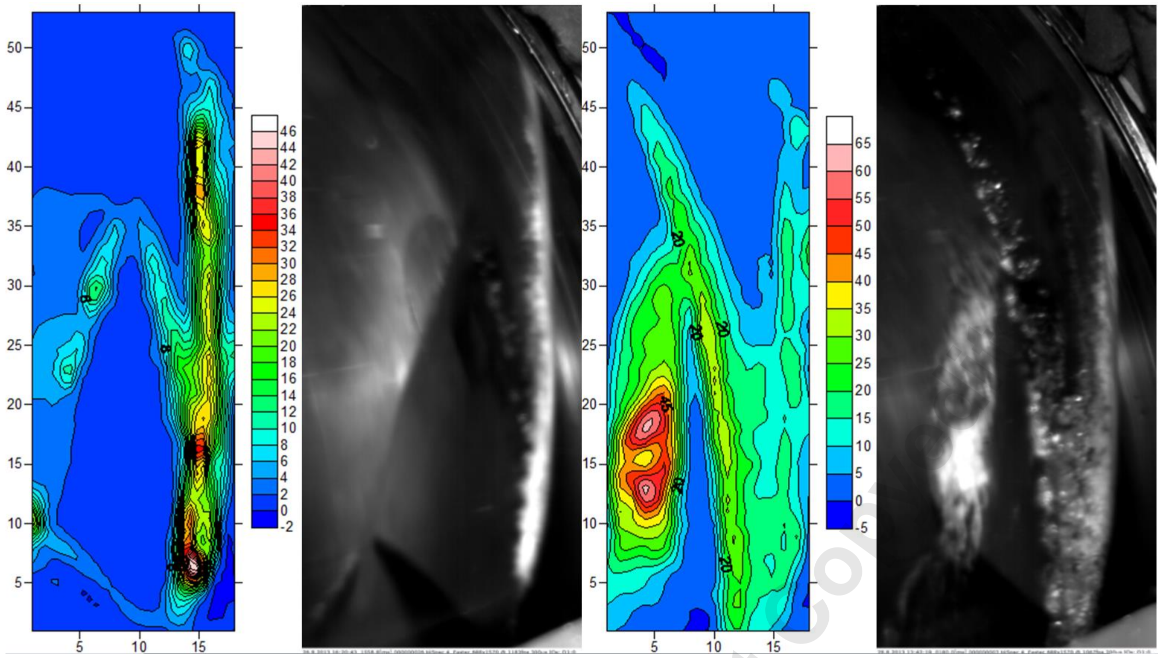

Figure 17: Standard deviation S and time averaged greyscale intensity $\langle \mathrm{A(k,t)} \rangle$ *of cavitation structures for modified runner (left at σ = 1.6) and unmodified runner (right at σ = 1.9) at operating point (*ψ_5 *= 0.206 and φ = 0.305)*

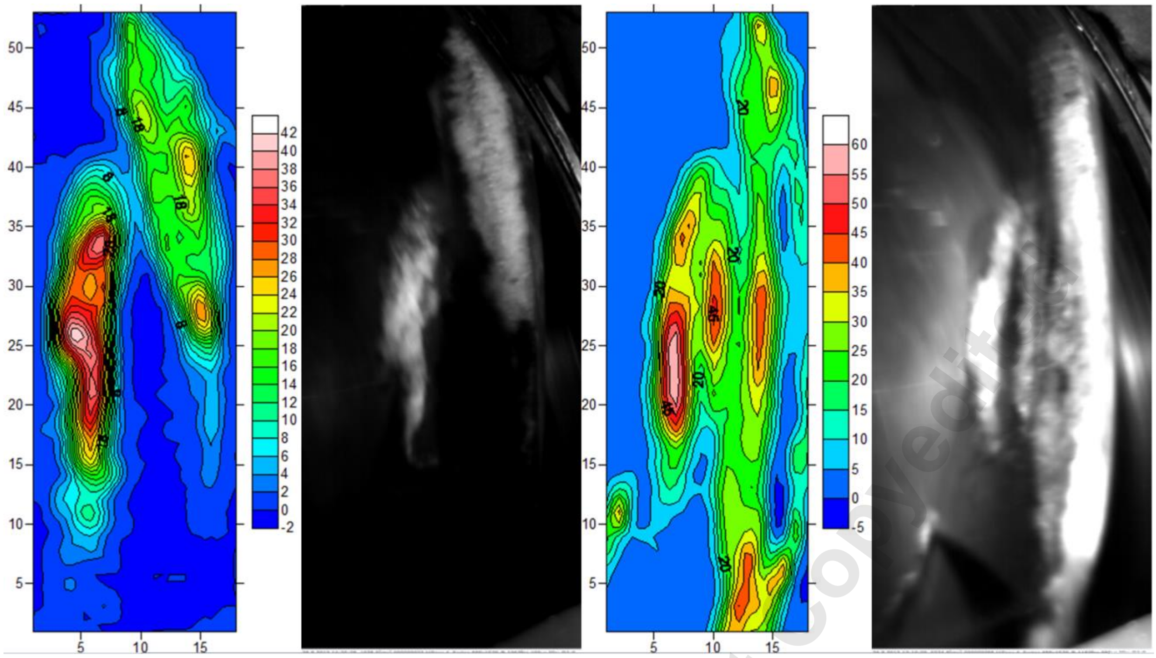

Figure 18: Standard deviation S and time averaged greyscale intensity $\langle A(k,t)\rangle$ *of cavitation structures for modified runner (left at σ = 0.7) and unmodified runner (right at σ = 1.0) at operating point (*ψ_6 *= 0.4034 and φ = 0.313)*

Journal of Fluids Engineering. Received October 11, 2017;
Accepted manuscript posted November 15, 2018. doi:10.1115/1.4041985

Table 1: Turbine blade profiles characteristics

PARAMETERS	UNMODIFIED PROFILE	MODIFIED PROFILE
Profile chord length L	*1 L*	*1 L*
Maximum profile thickness d_{max}	0.0425 *L*	0.0425 *L*
Position of maximum thickness l_1	0.15 *L*	0.4 *L*
Ratio l_1/l	15%	40%
Maximum profile curvature s_{max}	0.0145 *L*	0.0145 *L*
Position of maximum curvature l_2	0.3 *L*	0.45 *L*
Ratio l_2/l	30%	45%
Leading edge radius r_0	0.009 *L*	0.007 *L*

Journal of Fluids Engineering. Received October 11, 2017;
Accepted manuscript posted November 15, 2018. doi:10.1115/1.4041985

Table 2: Kaplan runner blades dimensional characteristics

PARAMETER	MODIFIED BLADE	UNMODIFIED BLADE
Nominal runner diameter D_0	ø 350mm	ø 350mm
Number of runner blades Z	4	4
Location of reference hydrofoil R_h	95% D_0	95% D_0
Blade angle β_0	25 °	25 °
Blade chord line length at 95 % R	180.70 mm	180.70 mm
Location of maximum thickness l_1	27.11 mm	72.28 mm
Ratio l_1/l	15 %	40 %
location of maximum curvature l_2	54.20 mm	81.30 mm
Ratio l_2/l	30 %	45 %
Leading edge radius r_0	1.63 mm	1.27 mm

NOMENCLATURE

$A(k,t)$ spatially averaged grey level intensity

A_0 guide vane opening coefficient

a_v minimal distance between two guide vanes

D nominal diameter of turbine

D_v centre of guide vanes pivot diameter

E specific energy of the turbine

$E(i,j,t)$ local grey level intensity

g gravity of earth

H_s suction head

k observation window

N turbine rotational speed

$NPSE$ Net Positive Suction Energy

p fluid pressure

p_{abs2} absolute pressure at draft tube outlet section

P_M mechanical power

p_{va} pressure of water evaporation

Q volume flow rate

R radius

S standard deviation of averaged grey level intensity

t time step

Journal of Fluids Engineering. Received October 11, 2017;
Accepted manuscript posted November 15, 2018. doi:10.1115/1.4041985

v velocity

v_2 water velocity at draft tube outlet section

z height of the streamline above a reference level

z number of guide vanes

z_2 level at draft tube outlet section

z_r reference constant level

β blade angle

η_T efficiency

ρ water density

σ cavitation number

σ_0 cavitation number of measurable influence on turbine efficiency

σ_{-1} cavitation number of turbine efficiency drop for more than 1%

σ_i incipient cavitation number

σ_{pl} cavitation number of the plant

φ flow rate number

ψ energy number

REFERENCES

[1] Brandi, R. B. S., Ramos, T. P., David, P. A. M. S., Dias B. H., da Silva Junior I. C ., Marcato, A. L. M., 2016, Maximizing hydro share in peak demand of power systems long-termoperation planning. Electr Power Syst Res, vol 41, pp. 264–271.

[2] Egre, D., Milewski, J.C., 2002, The diversity of hydropower projects, Energy Policy, Vol. 30, no. 14, pp. 1225-1230.

[3] Bajcar, T., Širok, B., Eberlinc, M., 2009, Quantification of Flow Kinematics Using Computer-Aided Visualization, Strojniški vestnik - Journal of Mechanical Engineering, vol. 55, no. 4, pp. 215-223

[4] Rus, T., Dular, M., Širok, B., Hočevar, M., Kern, I., 2007, An investigation of the relationship between acoustic emission, vibration, noise and cavitation structures on a Kaplan turbine. Journal of fluids engineering: Transactions of the ASME, vol. 129, no. 9, pp. 1112-1122.

[5] Cenčič, T., Hočevar, M., Širok, B., 2014, Study of erosive cavitation detection in pump mode of pump-storage hydropower plant prototype. Journal of fluids engineering: Transactions of the ASME, vol. 136, no. 5, pp. 051301-1-051301-11.

[6] Širok, B., Dular, M., Stoffel, B., 2006, Kavitacija, Fakulteta za strojništvo, vol. 1, Ljubljana/Darmstadt, Slovenia.

[7] Eichler, O., Jaeger, E.-U., 1981, The assessment of the cavitation behavior of kaplan turbines on the basis of a comparison between model tests and field experience, Voith Research and Construction, vol. 25e, pp. 4.1-4.12.

[8] De Lucia, M., Anguzza G., 1994, Visualization and Image Processing To Study The Cavitation Process in Hydraulic Turbomachinery, Modelling, Testing & Monitoring for Hydro powerplants Conference papers, pp. 383-389, Budapest, Hungary.

[9] Stefanović, Z., 2005, Aeroprofili, Mašinski fakultet, Beograd, Serbia.

[10] Riegels, W., 1958, Aerodynamische profile, Oldenbourg, München, Germany.

[11] Kuethe, A. M., Schetzer, J. D., 1959, Foundations of Aerodynamics, second edition, department of Aeronautical Engineering, University of Michigan, USA.

[12] Avellan, F., 2004, Introduction to cavitation in hydraulic machinery, The 6th International Conference on Hydraulic Machinery and Hydrodynamics, Timisoara, Romania.

Journal of Fluids Engineering. Received October 11, 2017;
Accepted manuscript posted November 15, 2018. doi:10.1115/1.4041985

[13] International standard IEC 60193, Hydraulic Turbines, storage pumps and pump-turbines – Model acceptance tests, second edition, 1999, 1999-11, International Electrotechnical Commision.

[14] Measurement methods and equipment on turbine test rigs, 2010, Turboinštitut, Report No. 2646e, Ljubljana, Slovenia.

[15] Low pressure turbine test rig, Turboinštitut, 2010, Report No. 2299e, Ljubljana, Slovenia.

[16] Chanson, H., 2013, Advective Diffusion of Air Bubbles in Turbulent Water Flows, in "Fluid Mechanics of Environmental Interfaces", Taylor & Francis, Leiden, The Netherlands, editors Gualtieri, C., and Mihailovic, D.T. , Editors, 2nd edition, Chapter 7, pp. 181-219.

[17] Širok, B., Potočar, E., Novak, M., 2000, Analiza kinematike toka za utripajočim profilom spremenljive geometrijske oblike z uporabo računalniške vizualizacije, Strojniški vestnik, vol. 46, pp. 330-341, Ljubljana, Slovenia.

[18] Brennen, C.E., 1994, Cavitation and Bubble Dynamics, Oxford University Press, Inc., New York.

[19] Rus, T., Dular, M., Širok, B., Hočevar, M., Kern, I., 2007, An investigation of the relationship between acoustic emission, vibration, noise and cavitation structures on a Kaplan turbine, Journal of fluids engineering: Transactions of the ASME, vol. 129, no. 9, pp. 1112-1122.

Figure Captions List

Journal of Fluids Engineering. Received October 11, 2017;
Accepted manuscript posted November 15, 2018. doi:10.1115/1.4041985

cavitation structures for modified runner (left at σ = 1.2) and unmodified runner (right at σ = 1.5) at operating point (ψ_2 = 0.2857 and φ = 0.31)

Fig. 15 *Standard deviation S and time averaged greyscale intensity* $\langle \mathrm{A(k,t)} \rangle$ *of cavitation structures for modified runner (left at σ = 1.3) and unmodified runner (right at σ = 1.6) at operating point (ψ_3 = 0.252 and φ = 0.318)*

Fig. 16 *Standard deviation S and time averaged greyscale intensity* $\langle \mathrm{A(k,t)} \rangle$ *of cavitation structures for modified runner (left at σ = 2.0) and unmodified runner (right at σ = 2.4) at operating point (ψ4 = 0.1513 and φ = 0.30)*

Fig. 17 *Standard deviation S and time averaged greyscale intensity* $\langle \mathrm{A(k,t)} \rangle$ *of cavitation structures for modified runner (left at σ = 1.6) and unmodified runner (right at σ = 1.9) at operating point (ψ_5 = 0.206 and φ = 0.305*

Fig. 18 *Standard deviation S and time averaged greyscale intensity* $\langle A(k,t) \rangle$ *of cavitation structures for modified runner (left at σ = 0.7) and unmodified runner (right at σ = 1.0) at operating point (ψ_6 = 0.4034 and φ = 0.313)*

Journal of Fluids Engineering. Received October 11, 2017;
Accepted manuscript posted November 15, 2018. doi:10.1115/1.4041985

Table Caption List